

ICEMG 2023-XXXXX

## Three-Dimensional Thermal Analysis of a Rotor-Excited Axial Flux Switching Permanent Magnet Machine by Computational Fluid Dynamics Method

Pedram Dehgoshaei<sup>1</sup>, Ali Zarghani<sup>2</sup>, Hossein Torkaman<sup>3</sup>, Aghil Ghaheri<sup>4</sup>

<sup>1</sup>Department of Electrical Engineering, Shahid Beheshti University, Tehran, Iran; pedram.dehi@yahoo.com

<sup>2</sup>Department of Electrical Engineering, Shahid Beheshti University, Tehran, Iran; A.zarghani@mail.sbu.ac.ir

<sup>3</sup>Department of Electrical Engineering, Shahid Beheshti University, Tehran, Iran; h\_torkaman@sbu.ac.ir

<sup>4</sup>Department of Electrical Engineering, Shahid Beheshti University, Tehran, Iran; A\_ghaheri@sbu.ac.ir

### Abstract

During conversation energy by electric machines, some energy will inevitably be wasted in the form of losses. The machine losses will be converted into heat and will increase the temperature of the machine components. Due to the dependence of electrical and mechanical properties of materials on temperature, investigating the heat transfer process in electric machines is imperative. This paper performs thermal analysis of a 2.3 kW, totally enclosed, rotor-excited axial flux switching permanent magnet (RE-AFSPM) machine for electric vehicle application by computational fluid dynamics method. Electromagnetic analysis based on the three-dimensional finite element method has been conducted to calculate losses accurately. Steady-state components temperature has been evaluated under nominal operating conditions, various rotational speeds, and different external convection coefficients. In addition, inserting blades for cooling performance of the RE-AFSPM are developed. Besides, temperature control along with the effect of the housing material on the component's temperature has been investigated. Results indicate utilizing aluminum housing, the RE-AFSPM have better thermal performance rather than cast iron.

**Keywords:** thermal analysis, cooling system, computational fluid dynamics, axial flux permanent magnet machine, electric vehicle.

### Introduction

In recent years, axial flux permanent magnet (AFPM) machines have been widely used due to significant advantages such as high torque density, simple structure, high efficiency, high reliability, and easy integration with other mechanical components [1]. As a result, AFPM machines are used in various applications, such as electric vehicles [2, 3], electric aircraft [4], wind turbines [5], and electric ship propulsion [6].

As the temperature increases, the coil resistance and the copper losses rise which reduces the efficiency and weakens the windings insulation. Also, remanent flux density and corrective force of a permanent magnet (PM) decrease as temperatures increases. Thus, PM strength degrades and the torque density of PM machines will reduce [7]. Extensive research has been focused on the thermal analysis of radial flux electric machines. In contrast, less attention has been paid to the thermal analysis of AFPMS [8]. Because the internal heat flow of AFPMS is completely different from radial flux machines, thermal analysis of AFPMS is of particular importance

[9]. In a thermal analysis of electric machines, the analytical method of lumped parameter thermal network (LPTN) and numerical approaches such as finite element method (FEM) and computational fluid dynamics (CFD) are widely used. FEM is highly accurate in modeling conduction heat transfer [10]. However, with CFD, more realistic modeling of airflow in the machine can be performed, leading to advanced heat transfer investigation by convection from machine components to the cooling. CFD is widely used to calculate convection coefficients [11], air ventilation modeling, and cooling systems analysis [12, 13]. In [13], through CFD-based simulation, it was proved that by inserting copper bars as additional heat transfer paths between the stator teeth and the liquid cooling chamber in the end shield, the temperature could be reduced by up to 15%. The behavior of the internal fluid depends on the machine's structure. So, the results of the thermal analysis of a machine cannot be generalized to another machine with a different topology. Therefore, in this paper, the steady-state thermal analysis has been performed by the CFD method for a 2.3 kW rotor-excited axial flux switching permanent magnet (RE-AFSPM) machine. Against other type of AFPMS where PMs are located on the rotor disk surface [14-16], in RE-AFSPM the rotor is segmented and PMs are sandwiched between the rotor segments. To accurately calculate the losses, the three-dimensional (3-D) FEM has been used. The RE-AFSPM is housed in a totally enclosed chamber with blades for better heat transfer. Thermal analysis for the chamber is evaluated with two materials of aluminum and cast iron. Also, the thermal performance of these materials is studied. The effect of the convection heat transfer coefficient on the temperature difference of the machines' components has been investigated. Finally, the influence of rotational speed and the current density on temperature distribution is examined.

### Topology, Electromagnetic, and Thermal Analysis of the RE-AFSPM Machine

In this section, the studied AFPM motor is introduced, then the electromagnetic analysis will be performed to calculate the losses and a thermal study will be defined.

#### Machine Topology

The 3-D geometry of the RE-AFSPM machine, first developed in [2], is shown in Fig. 1. The structure consists of two separate segmented rotors, a double-sided stator, concentrated windings, housing, and PMs. The housing is equipped with blades for better cooling.

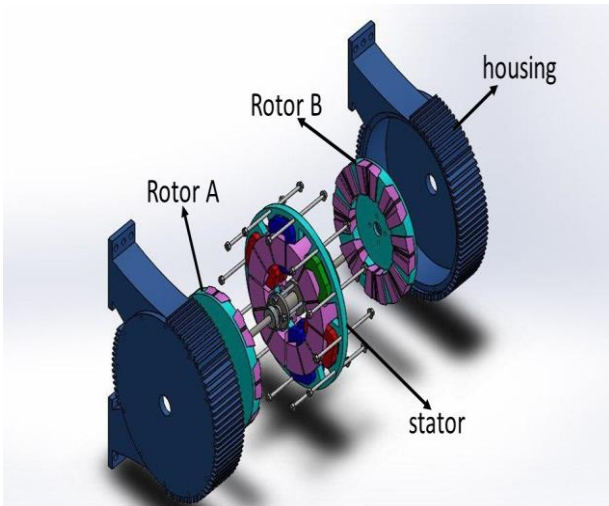


Fig. 1. Exploded 3-D view of the RE-AFSPM machine

As depicted in Fig. 2, a hole is created between the 8 poles of the rotor where the PMs are placed in the space between the rotor segments. The rotor segments and PMs are situated firmly in the rotor frame.

For a better conception, the stator core is pictured in Fig. 3. The stator consists of 6 main poles and 6 auxiliary poles with concentrated coils wrapped around the main poles. Also, support is utilized to maintain the stator in place.

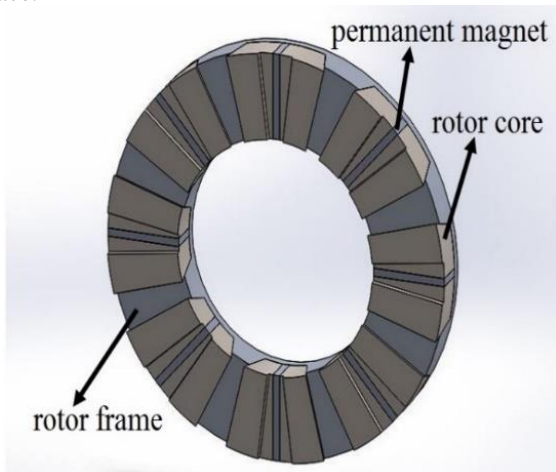


Fig. 2. Structure of rotating components of the RE-AFSPM

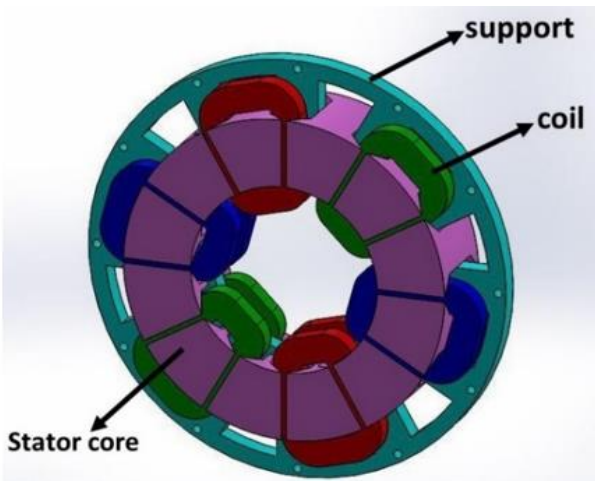


Fig. 3. Stator and winding arrangement of the RE-AFSPM

## Electromagnetic Analysis

Since the losses calculation with mathematical correlations through the analytical method requires the consideration of many assumptions and its accuracy is low, the FEM is used to accurately and automatically derive electromagnetic losses [17]. As the flux path in the RE-AFSPM is in axial, radial, and circumferential directions, a 3-D model has been accomplished to increase the analysis accuracy. The machine nominal specifications are listed in Table 1.

To create a thermal analysis, it is necessary to determine the material's properties including density, specific heat capacity, and thermal conductivity. The thermal characteristics of the materials used in the RE-AFSPM are given in Table 2.

Losses produce heat and cause rising the components temperature. Thus, to perform thermal analysis, firstly it is necessary to calculate the power losses. In general, losses occur in the rotor core, stator core, PMs and winding. Because the RE-AFSPM operates in low-speeds, mechanical losses can be ignored. Power losses in machine components at speeds of 500 rpm to 1000 rpm are illustrated in Fig. 4. It is observed that the electromagnetic losses of the stator core, rotor core, rotor frame and PM increase in proportion to the speed, but copper losses are constant. For example, by increasing the machine speed from 500 rpm to 1000 rpm, the stator core losses have raised by 2.1, the rotor core losses by 2.35 and the rotor frame losses by 1.9 times.

Table 1. RE-AFSPM machine nominal specifications

Parameter	Value	Unit
Rated Power	2.3	kW
Rated speed	500	rpm
Rated current	7	A
Phase number	3	-
Air-gap length	0.5	mm
PM width	5	mm
Total axial length	103	mm

Table 2. Thermal properties of the RE-AFSPM components

Component (material)	Thermal conductivity ( $\frac{W}{m \cdot ^\circ C}$ )	Specific heat ( $\frac{J}{kg \cdot ^\circ C}$ )	Density ( $\frac{kg}{m^3}$ )
Winding (copper)	386	380	8954
Support & Rotor frame (aluminum)	237	903	2700
Fluid (air)	0.024	1006	1.225
Frame (cast iron)	55	456	7920
PM (Nd-Fe-B)	8.95	501.6	7500
Stator & Rotor core (50JN400)	30	450	7650
Shaft (S45C)	49.8	486	7850

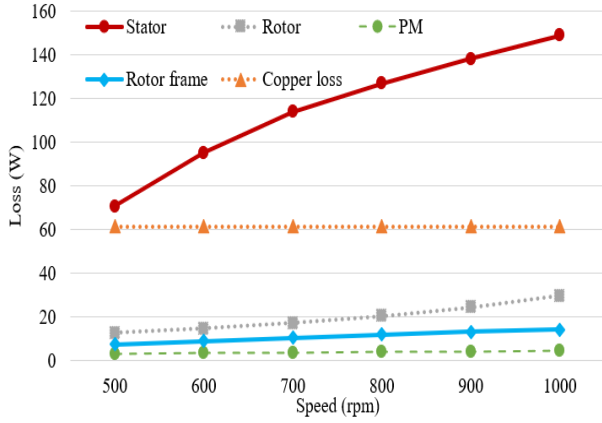


Fig. 4. Power losses of components versus the speed

### Thermal Analysis

In this sub-section, Ansys Fluent software, one of the most powerful CFD software, has been used to perform thermal analysis of the RE-AFSPM with a high accuracy. Because the losses cause heat, the nominal losses calculated in the previous section are injected into the steady-state thermal analysis. The ambient temperature is set at 50 °C to create the most difficult operating conditions. The steady-state analysis compares the temperature distribution for the two types of housing made of aluminum and cast iron. Thermal analysis has also been performed for speeds from 500 rpm to 1000 rpm. The assumptions made for the air-fluid are as follows:

- Newtonian fluid.
- Compressible fluid.
- Non-slip conditions.
- Fixed properties.

Equations (1) to (5) express the equations of conservation, continuity, momentum and energy in a fluid, respectively:

$$\frac{\partial u}{\partial x} + \frac{\partial v}{\partial y} + \frac{\partial w}{\partial z} = 0 \quad (1)$$

$$\rho_f \left( u \frac{\partial u}{\partial x} + v \frac{\partial u}{\partial y} + w \frac{\partial u}{\partial z} \right) = -\frac{\partial P}{\partial x} + \mu_f \left( \frac{\partial^2 u}{\partial x^2} + \frac{\partial^2 u}{\partial y^2} + \frac{\partial^2 u}{\partial z^2} \right) \quad (2)$$

$$\rho_f \left( u \frac{\partial v}{\partial x} + v \frac{\partial v}{\partial y} + w \frac{\partial v}{\partial z} \right) = -\frac{\partial P}{\partial y} + \mu_f \left( \frac{\partial^2 v}{\partial x^2} + \frac{\partial^2 v}{\partial y^2} + \frac{\partial^2 v}{\partial z^2} \right) \quad (3)$$

$$\rho_f \left( u \frac{\partial w}{\partial x} + v \frac{\partial w}{\partial y} + w \frac{\partial w}{\partial z} \right) = -\frac{\partial P}{\partial z} + \mu_f \left( \frac{\partial^2 w}{\partial x^2} + \frac{\partial^2 w}{\partial y^2} + \frac{\partial^2 w}{\partial z^2} \right) \quad (4)$$

$$\rho_f C_{pf} \left( u \frac{\partial T_f}{\partial x} + v \frac{\partial T_f}{\partial y} + w \frac{\partial T_f}{\partial z} \right) = k_f \left( \frac{\partial^2 T_f}{\partial x^2} + \frac{\partial^2 T_f}{\partial y^2} + \frac{\partial^2 T_f}{\partial z^2} \right) \quad (5)$$

where  $P$  is the pressure,  $\rho_f$  is the fluid density,  $\mu_f$  is the fluid absolute viscosity,  $C_{pf}$  is the fluid specific heat capacity, and  $k_f$  is the thermal conductivity of the fluid. The energy equation for a solid body is as follows:

$$\rho_s C_{ps} \frac{\partial T_s}{\partial t} = k_s \left( \frac{\partial^2 T_s}{\partial x^2} + \frac{\partial^2 T_s}{\partial y^2} + \frac{\partial^2 T_s}{\partial z^2} \right) + \dot{q} \quad (6)$$

where  $\rho_s$  is the solid density,  $C_{ps}$  is the solid specific heat,  $k_s$  is the solid thermal conductivity, and  $\dot{q}$  is the rate of solid heat production. The convection heat transfer relationship to calculate the amount of heat flux from the machine surface to the outside environment is as follows:

$$-k \frac{\partial T}{\partial x} = h_{out} (T_{S_{out}} - T_{f_{out}}) \quad (7)$$

where  $T_{S_{out}}$  is the outer surface temperature of the machine,  $T_{f_{out}}$  is temperature of the ambient, and  $h_{out}$  is the convection heat transfer coefficient. In this research, simulations have been performed for  $h_{out}$  values equal to 10, 20, 40 and 80  $\frac{w}{m^2k}$ . The convergence requirement for the energy equation and the coherence for the iterations to reach the remainder are  $10^{-6}$  and  $10^{-3}$ , respectively.

### Simulation Results

Considering  $h_{out} = 10 w/(m^2k)$  and ambient temperature of 50 °C, the temperature distribution of the RE-AFSPM at 500 rpm with aluminum housing and a cast iron housing is shown in Fig. 5. In the case of an aluminum housing, the temperature range of machine parts is 136 °C to 187 °C. For cast iron housing with similar conditions, the temperature range is 137 °C to 191 °C. As a comparison, using an aluminum housing, the temperature of the internal fluid in the vicinity of the housing and the rotating components temperature have also been reduced to 6%. Therefore, it can be concluded that the heat transfer of aluminum housing is better than cast iron, and more heat dissipation is achieved by an aluminum housing. According to the temperature distribution along with the plane  $Y = 0$  and  $Z = 0$ , Fig. 5 manifests that the coils are the hottest part of the machine and the rotor segments temperature is lower than the stator core and coil. Because the rotor losses is less than the stator and copper loss, the low rotor temperature was expected.

In addition, the temperature distribution for aluminum housing case at ambient temperature of 300 K and rotational speed of 500 rpm where  $h_{out} = 10 w/(m^2k)$  is studied. Fig. 6 exhibits the temperature distribution for this scenario. Comparing Fig. 5 and Fig. 6 shows that with a decrease in the ambient temperature by 46%, the machine maximum temperature decreases approximately 14%.

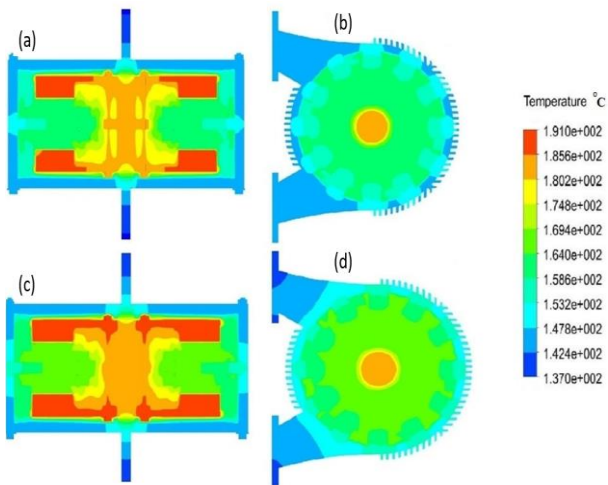


Fig. 5. Temperature distribution at 500 rpm with ambient temperature 50 °C for aluminum housing in (a) plane Y=0, (b) plane Z=0; For cast iron housing in (c) plane Y=0 and (d) plane Z=0

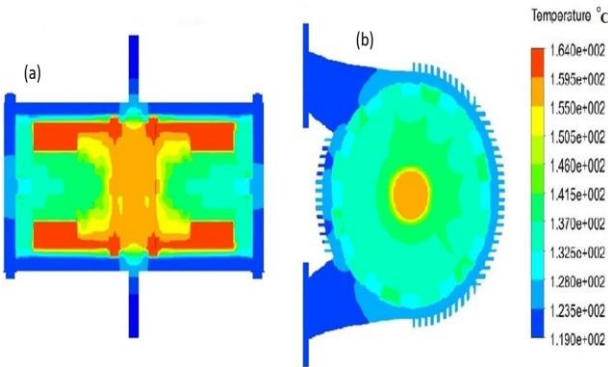


Fig. 6. Temperature distribution per velocity 500 rpm and  $h_{out} = 10 \frac{w}{m^2k}$  with an ambient temperature of 300 K in (a) plane Y=0 and (b) plane Z=0

To investigate the effect of outer convection coefficient on the temperature of machine components, simulation is conducted for various values of outer convection coefficients such as  $h_{out} = 20 \frac{w}{m^2k}$ ,  $h_{out} = 40 \frac{w}{m^2k}$ , and  $h_{out} = 80 \frac{w}{m^2k}$  with the aluminum housing at the ambient temperature of 300 K. The results of the temperature distribution on the planes Y=0 and Z=0 are depicted in Fig. 7. Comparing the results, it can be observed with increasing the value of  $h_{out}$ , the temperature of the machine components also decreased due to the greater effect of the fluid on the heat dissipation. For example, for  $h_{out} = 20 \frac{w}{m^2k}$  the temperature range is 66 °C to 116 °C. However, in the case of  $h_{out} = 10 \frac{w}{m^2k}$ , as shown in Fig. 6, the temperature range was 119 °C to 164 °C. Therefore, it can be concluded that by doubling  $h_{out}$ , the maximum temperature of the machine has decreased by 29%. Also in  $h_{out} = 40 \frac{w}{m^2k}$  scenario, the temperature range is 44 °C to 92 °C and for  $h_{out} = 80 \frac{w}{m^2k}$  the temperature range is 33 °C to 80 °C. Therefore, in the case of  $h_{out} = 20 \frac{w}{m^2k}$ ,  $h_{out} = 40 \frac{w}{m^2k}$ , and  $h_{out} = 80 \frac{w}{m^2k}$ , the temperature decreased by 29%, 43.9% and 51%, respectively, compared to  $h_{out} = 10 \frac{w}{m^2k}$ .

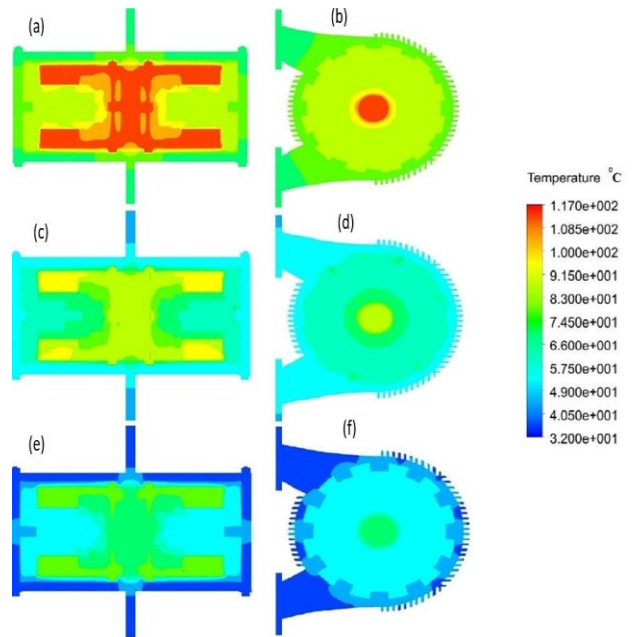


Fig. 7. Temperature distribution at ambient temperature of 300 K for (a-b):  $h_{out} = 20 \frac{w}{m^2k}$ , (c-d):  $h_{out} = 40 \frac{w}{m^2k}$  and (e-f):  $h_{out} = 80 \frac{w}{m^2k}$

In the next scenario, simulations are performed for the speeds from 500 rpm to 1000 rpm. In this case, the ambient temperature is set to 300 K,  $h_{out} = 10 \frac{w}{m^2k}$  and the machine is equipped with aluminum housing. The temperature distribution is displayed in Fig. 8. Due to the dependence of losses on the machine rotational speed, the losses increase with increasing speed in different parts. Therefore, more heat is generated in different parts, which causes the temperature of the machine components to increase. As the machine speed increased from 500 rpm to 1000 rpm, the component temperatures increased by 60%.

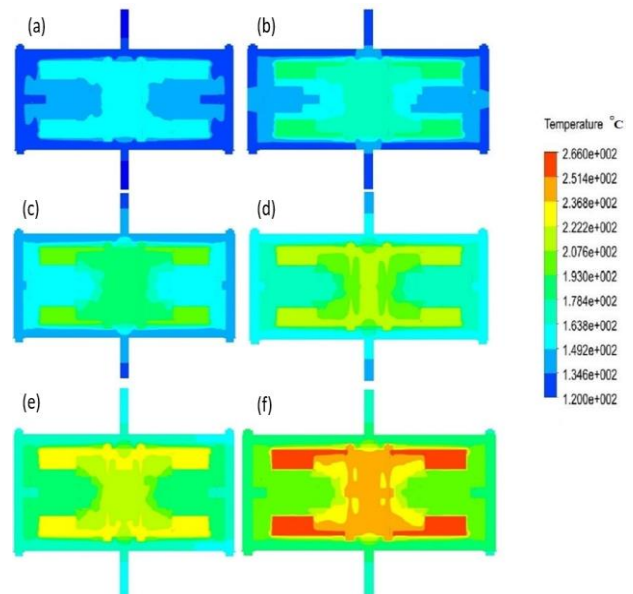


Fig. 8. Temperature distribution at ambient temperature of 300 K and  $h_{out} = 10 \frac{w}{m^2k}$  on plane Y=0 for (a) 500 rpm, (b) 600 rpm, (c) 700 rpm, (d) 800 rpm, (e) 900 rpm, and (f) 1000 rpm

Finally, because the torque density varies with current density, it is necessary to perform a thermal analysis. As the current density increases, the copper losses increase dramatically. Convection coefficients are independent from current density. Therefore, as the current density increases, the losses increase, and more heat is generated in the machine, increasing the temperature in all machine components, especially the windings. Although the average torque increases by 45% as the current density rises from 3.6 A/mm<sup>2</sup> to 6.3 A/mm<sup>2</sup>, the PM temperature increases by 84% and the winding temperature by 98%. Comparing the average temperature of machine components in Fig. 9 shows that the temperature of machine components increases with increasing current density. Also, results prove that the utilization of aluminum housing leads to a lower temperature in machine components than cast-iron housing.

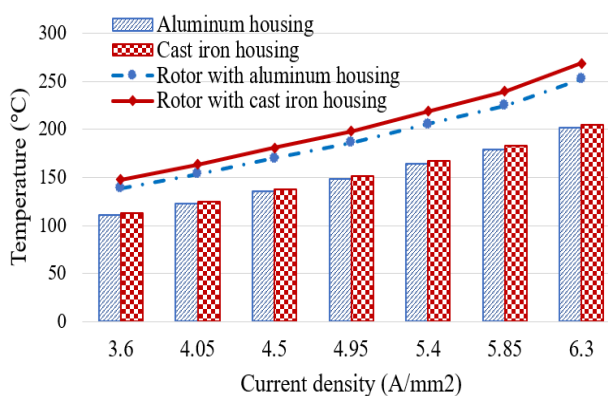


Fig. 9. Comparison of average rotor and housing temperature for the housing made of aluminum and cast iron

## Conclusion

This paper performed the thermal analysis of a RE-AFSPM machine using the CFD method for the first time. In order to improve heat transfer, blades were used on the machine housing to increase the level of contact with the ambient and reduce the machine components temperature. In the case of aluminum housing compared to cast-iron housing, the rotor temperature reduced as 6%. Therefore, the heat transfer of aluminum housing is better than the cast iron. Comparing the results of varying ambient temperature, it was concluded that with 46% reduction of the ambient temperature, the maximum temperature is reduced by 14%. Also, the effect of the outside convection coefficient variation on the components temperature was investigated. It was obtained that for maximum convection coefficients equal to  $20 \frac{w}{m^2k}$ ,  $40 \frac{w}{m^2k}$ , and  $80 \frac{w}{m^2k}$ , the maximum machine temperature decreased by 29%, 43.9% and 51%, respectively, compared to  $10 \frac{w}{m^2k}$ . As the machine speed increased, the temperature of the various parts raised considerably due to the increase in power losses. As the machine speed doubled, the components temperature increased by up to 60%. Finally, by varying current density, it proved that utilizing aluminum housing instead of cast iron, lower temperature of components can be achieved.

## References

- [1] L. Shao, R. Navaratne, M. Popescu, and G. Liu, "Design and construction of axial-flux permanent magnet motors for electric propulsion applications—A review," *IEEE Access*, 2021.
- [2] H. Torkaman, A. Ghaheri, and A. Keyhani, "Design of rotor excited axial flux-switching permanent magnet machine," *IEEE Transactions on Energy Conversion*, vol. 33, no. 3, pp. 1175-1183, 2018.
- [3] W. Geng, Y. Wang, J. Wang, J. Hou, J. Guo, and Z. Zhang, "Comparative Study of Yokeless Stator Axial-Flux PM Machines having Fractional Slot Concentrated and Integral Slot Distributed Windings for Electric Vehicle Traction Applications," *IEEE Transactions on Industrial Electronics*, vol. 70, no. 1, pp. 155-166, 2022.
- [4] Z. Zhang, W. Geng, Y. Liu, and C. Wang, "Feasibility of a new ironless-stator axial flux permanent magnet machine for aircraft electric propulsion application," *CES Transactions on Electrical Machines and Systems*, vol. 3, no. 1, pp. 30-38, 2019.
- [5] A. Daghigh, H. Javadi, and H. Torkaman, "Design optimization of direct-coupled ironless axial flux permanent magnet synchronous wind generator with low cost and high annual energy yield," *IEEE Transactions on Magnetics*, vol. 52, no. 9, pp. 1-11, 2016.
- [6] P. Ojaghu and A. Vahedi, "Specification and design of ring winding axial flux motor for rim-driven thruster of ship electric propulsion," *IEEE Transactions on Vehicular Technology*, vol. 68, no. 2, pp. 1318-1326, 2018.
- [7] M. Chen, W. Hua, and G. Zhao, "Thermal performance of a flux-switching permanent magnet machine for an integrated starter generator in hybrid electric vehicles," in *Proc. Int. Conf. Electr. Mach. Syst.*, Aug. 2017, pp. 1-6.
- [8] A. Boglietti, A. Cavagnino, D. Staton, M. Shanel, M. Mueller, and C. Mejuto, "Evolution and modern approaches for thermal analysis of electrical machines," *IEEE Transactions on Industrial Electronics*, vol. 56, no. 3, pp. 871-882, 2009.
- [9] D. A. Howey, P. R. Childs, and A. S. Holmes, "Air-gap convection in rotating electrical machines," *IEEE Transactions on Industrial Electronics*, vol. 59, no. 3, pp. 1367-1375, 2010.
- [10] A. Zarghani, H. Torkaman, N. Arbab, and M. S. Toulabi, "Lumped parameter thermal network for thermal analysis of a rotor-excited axial flux switching machine with electromagnetic-thermal design," *Measurement*, vol. 193, no. 2022, pp. 1-16, 2022.
- [11] A. Rasekh, P. Sergeant, and J. Vierendeels, "Fully predictive heat transfer coefficient modeling of an axial flux permanent magnet synchronous machine with geometrical parameters of the magnets," *Applied Thermal Engineering*, vol. 110, pp. 1343-1357, 2017.
- [12] W. Yu, W. Hua, and Z. Zhang, "Cooling Analysis of High-Speed Stator-Permanent Magnet Flux-Switching Machines for Fuel-Cell Electric Vehicle

- Compressor," *IEEE Trans. Vehicular Techn.*, vol. 71, no. 1, pp. 210-219, 2021.
- [13] Y. C. Chong, E. J. E. Subiabre, M. A. Mueller, J. Chick, D. A. Staton, and A. S. McDonald, "The ventilation effect on stator convective heat transfer of an axial-flux permanent-magnet machine," *IEEE Transactions on Industrial Electronics*, vol. 61, no. 8, pp. 4392-4403, 2013.
- [14] D. A. Howey, A. S. Holmes, and K. R. Pullen, "Measurement and CFD prediction of heat transfer in air-cooled disc-type electrical machines," *IEEE Transactions on Industry Applications*, vol. 47, no. 4, pp. 1716-1723, 2011.
- [15] L. Veg and J. Laksar, "Comparison of two types of cooling of axial flux permanent magnet machines by CFD simulation," in *2019 International Conference on Electrical Drives & Power Electronics (EDPE)*, 2019: IEEE, pp. 303-306.
- [16] J. Li, Y. Lu, Y.-H. Cho, and R. Qu, "Design, analysis, and prototyping of a water-cooled axial-flux permanent-magnet machine for large-power direct-driven applications," *IEEE Transactions on Industry Applications*, vol. 55, no. 4, pp. 3555-3565, 2019.
- [17] R. Nasiri-Zarandi, A. Ghaheri, and K. Abbaszadeh, "Thermal modeling and analysis of a novel transverse flux HAPM generator for small-scale wind turbine application," *IEEE Transactions on Energy Conversion*, vol. 35, no. 1, pp. 445-453, 2019.